Cu_2ZnSnS_4-Ag_2S Nanoscale P-N Heterostructures as Sensitizers for Photoelectrochemical Water Splitting

Xuelian Yu,[a,b] Jingjing Liu,[c] Aziz Genç,[d] Maria Ibáñez,[b] Zhishan Luo,[b] Alexey Shavel,[b] Jordi Arbiol,[d, e] Guangjin Zhang,[c] Yihe Zhang[a] and Andreu Cabot*[b,e]*

a. Beijing Key Laboratory of Materials Utilization of Nonmetallic Minerals and Solid Wastes, National Laboratory of Mineral Materials, School of Materials Science and Technology, China University of Geosciences, 100083, Beijing, P. R. China

b. Catalonia Energy Research Institute - IREC, 08930, Sant Adria del Besos, Barcelona, Spain

c. Key Laboratory of Green Process and Engineering, Chinese Academy of Sciences,100190, Beijing, P. R. China

d. Institut Català de Nanociència i Nanotecnologia, ICN2, Campus de la UAB, 08193 Bellaterra, Spain

e. Institució Catalana de Recerca i Estudis Avançats - ICREA, 08010, Barcelona, Spain

Cu_2ZnSnS_4-Ag_2S Nanoscale p-n Heterostructures as Sensitizers for Photoelectrochemical Water Splitting

ABSTRACT A cation exchange-based route was used to produce Cu_2ZnSnS_4(CZTS)-Ag_2S nanoparticles with controlled composition. We report a detailed study of the formation of such CZTS-Ag_2S nano-heterostructures and of their photocatalytic properties. When compared to pure CZTS, the use of nanoscale p-n heterostructures as light absorbers for photocatalytic water splitting provides superior photocurrents. We associate this experimental fact to a higher separation efficiency of the photogenerated electron–hole pairs. We believe this and other type-II nano-heterostructures will open the door to the use of CZTS, with excellent light absorption properties and made of abundant and environmental friendly elements, to the field of photocatalysis.

Introduction

Colloidal nanocrystals are highly suitable building blocks for the fabrication of energy conversion and storage devices. Their solution processability and the precise control that can be achieved over their chemical and structural parameters, which control their optical and electronic properties, make nanocrystal-based solution processing approaches highly advantageous when compared with conventional vacuum-based thin film technologies.[1-3,ACS Nano, 2015, 9, 1012–1057] However, current functional nanomaterials must meet too many very demanding properties not realizable with a unique compound. Thus the design of multicomponent nanostructures with improved, multiple and/or new physical-chemical properties, such as enhanced photoluminescence,[4-5] modified magnetic behavior,[6] improved (photo)catalytic performances,[7-9] and superior thermoelectric efficiencies,[10] is essential. In particular, p-n junction heterostructured nanoparticles provide new ways to manipulate electron and hole wave functions.[11] Among them, type-II nanoparticles, with a staggered alignment of band edges at the heterointerface, promote the spatial separation of electrons and holes.[12-15]

Several synthesis strategies have been developed to produce type-II nano-heterostructures. Among them, ion-exchange methods based on solubility constant difference have been proven as particularly suitable.[16] They provide versatility, high degree of control over composition of each compound, and high selectivity towards the formation of dimers with an epitaxial hetero-interface while keeping the geometry of the initial nanoparticles and preventing the nucleation of secondary phases.[17-18]

While most of the effort oriented to produce nanoheterostructures by cation exchange methods has been carried out with Cd-based chalcogenides, [19] very recently, this strategy has been also

applied to the total or partial conversion of more environmental friendly Cu-based chalcogenides.[20-22] Within this group of materials, a particularly environmental friendly direct band gap semiconductor is Cu_2ZnSnS_4 (CZTS). In the last decade, CZTS has attracted much attention in the field of thin film photovoltaics as alternative to CdTe and $CuIn_{1-x}Ga_xSe_2$. CZTS uniquely combines both, outstanding optoelectronic properties, and a composition based on elements that abundant in the Earth's crust. Particularly, its direct band gap at 1.5 eV matches well with the energy requirement for solar water splitting, what makes CZTS a strong candidate for water splitting.[23] However, in spite of its outstanding properties, and except for few examples on the photocatalytic generation of hydrogen and other value-added chemicals,[24-28] this material has been mostly ignored in the photocatalysis field. This is in part due to its high surface charge carrier recombination, which becomes critical in high surface area materials as those required for photocatalysis.

One solution to minimize recombination of photogenerated charge carriers is the rapid spatial separation of electrons and holes in heterostructures. CZTS and related quaternary nanocrystals can be nowadays produced by different synthetic approaches.[29-35] However, due to the difficulties in tuning the composition, phase, size and shape of such complex materials, the preparation of CZTS-based nanoscale p-n junction heterostructures still remains challenging.

In this work, we demonstrate that partial cation exchange is an excellent strategy to produce CZTS-based nanoheterostructures due to the high mobility of cations in the CZTS lattice. In particular, we describe the preparation of CZTS-based type-II nanoheterostructures via cation exchange of CZTS with Ag^+ ions to form CZTS-Ag_2S nanoparticles. The progressive exchange in the initial CZTS nanoparticles by Ag^+ ions allows controlling the relative ratio between the two compounds. We further demonstrate here that the use of CZTS-Ag_2S nano-heterostructures

as sensitizers provides significantly enhanced photocurrent response for photoelectrochemical water splitting under visible-light illumination.

Experimental

Chemicals and solvents

Tert-dodecylmercaptan, dodecanethiol, tin (IV) chloride ($SnCl_4 \cdot 5H_2O$), zinc oxide (ZnO), copper (II) chloride ($CuCl_2 \cdot 2H_2O$), silver nitrate ($AgNO_3$), 1-octadene (ODE), oleylamine (OLA, 70%), and oleic acid (OA, 90 %) were purchased from Aldrich. Chloroform, isopropanol, tetrahydrofuran (THF), toluene and methanol were of analytical grade and obtained from various sources. OLA was distilled before its use. The rest of the precursors and solvents where used without further purification.

Synthesis of CZTS-Ag_2S heterostructures

Quasi-spherical CZTS nanoparticles with wurtzite structure were prepared using the method we described before[25] by the reaction of copper, tin and zinc salts with a mixture of tert-dodecylmercaptan and dodecanethiol in the presence of OLA. In a typical synthesis, 5.4 mmol of $CuCl_2 \cdot 2H_2O$, 4.8 mmol of ZnO, and 1.8 mmol of $SnCl_4 \cdot 5H_2O$ were dissolved in THF. Then, 24 mmol of distilled OLA and 20 g of ODE were added to the reaction mixture. The solution was heated to 175 °C under argon flow and maintained at this temperature for 1 h. After purging, the mixture was cooled to 100 °C, and 50 mmol of tert-dodecylmercaptan and 5 mmol of dodecanethiol were added. The solution was then heated to 250 °C and kept for 1 h. The obtained CZTS nanocrystals were thoroughly purified by multiple precipitation and re-dispersion steps using 2-propanol and chloroform.

To produce CZTS-Ag_2S heterostructures, first, a stock precursor solution of $AgNO_3$ in OLA was made by dissolving 0.34 g $AgNO_3$ (2.0 mmol) in 10.0 mL OLA at 60 °C. Dissolution took ~15 min under magnetic stirring and N_2 atmosphere. When cooled down to room temperature, the colorless solution gradually turned into a white waxy paste. Then, 1 mL THF dispersion of the CZTS nanoparticles (~40 mg) was mixed with 10 mL ODE and 0.5 mL OLA under N_2 atmosphere. The solution was maintained under N_2 flow at 120 °C for 30 min to remove THF. Depending on the relative CZTS/Ag_2S ratio targeted, between 2 and 6 mL of $AgNO_3$ stock solution was quickly injected into the CZTS nanoparticle dispersion at 120 °C. The reaction was maintained at this temperature for 30 seconds before it was rapidly cooled down to room temperature using a water bath. Nanoparticles were finally washed by multiple precipitation and re-dispersion steps using toluene and ethanol.

Characterization techniques

The morphological, chemical and structural characterization of the nanoparticles was carried out by transmission electron microscopy (TEM) and high-resolution TEM (HRTEM). Carbon-coated TEM grids from Ted-Pella were used as substrates. HRTEM images were obtained using a JEOL 2010F field-emission gun microscope with a 0.19 nm point-to-point resolution at 200 keV with an embedded Gatan image filter for EELS analyses. Images were analyzed by means of Gatan Digital micrograph software.

Powder x-ray diffraction (XRD) patterns were obtained with Cu Kα (λ= 1.5406 Å) radiation in a reflection geometry on a Bruker D8 operating at 40 kV and 40 mA. UV-vis optical absorption spectra were recorded on a LAMBDA 950 UV-Vis spectrophotometer from PerkinElmer. X-ray

photoelectron spectroscopic (XPS) measurements were performed on a Thermo Scientific XPS spectrometer.

Photoelectrochemical response was measured using a CHI852C electrochemical workstation with conventional three-electrode setup under visible-light illumination. Fluorine doped tin oxide (FTO) glass substrates were cleaned with acetone and ethanol, and dried with pure nitrogen. To prepare the electrode, aqueous TiO_2 paste (25% w/w TiO_2, 10% w/w polyethylene glycol (MW 20 000)) was doctor bladed onto 1×1 cm^2 FTO substrates. The films were then calcined at 450 °C for 2 h. Then, the as-prepared CZTS-Ag_2S were first dispersed in 1 mL toluene with concentration of 1 mg/mL followed by sonication. After that, the solution was deposited on the working electrode substrate by spin-coating (rotation speed: 3,000 rpm). A platinum wire and Ag/AgCl were used as the counter and reference electrodes respectively. 0.1 M $Eu(NO_3)_3$ aqueous solution were used as electrolyte. The illumination source was a 300 W xenon lamp with a cut-off filter (λ>420 nm) to provide visible light illumination.

Results and Discussion

Figure 1a shows a representative TEM micrograph of the CZTS nanocrystals used to produce CZTS-based nanoheterostructures. CZTS nanocrystals were highly monodisperse, with an average size of 12±1 nm, and presented quasi-spherical geometries with faceted surfaces. CZTS-Ag_2S heterostructures were obtained by adding Ag^+ ions to a solution containing CZTS nanoparticles at 120 °C. CZTS-Ag_2S heterodimers were formed by the preferential cation exchange at the vertexes of the hexagonal structures, which are the most reactive sites (Figure 1b-d). A similar preferential partial cation exchange reaction was observed with CdS rods that

were progressively transformed into Cu_2S rods, starting at the nanorod tip as the most reactive regions.[JACS 2009, 131, 5285]

When increasing the amount of Ag^+ precursor added, the interface between the two compounds, CZTS and Ag_2S, moved inward the CZTS nanoparticle. The diameter of the Ag_2S nanocrystal increased from ~2 nm (Figure 1b, sample H1), to ~4 nm (Figure 1c, sample H2) and ~7 nm (Figure 1d, sample H3) when the amount of Ag^+ precursor used increased from 0.4 mmol, 0.8 mmol and 1.2 mmol, respectively. In accordance with the rapid kinetics characterizing cation exchange reactions,[36] the reaction was completed in less than 5 seconds and a further prolongation of the reaction time did not translate in any morphology change.

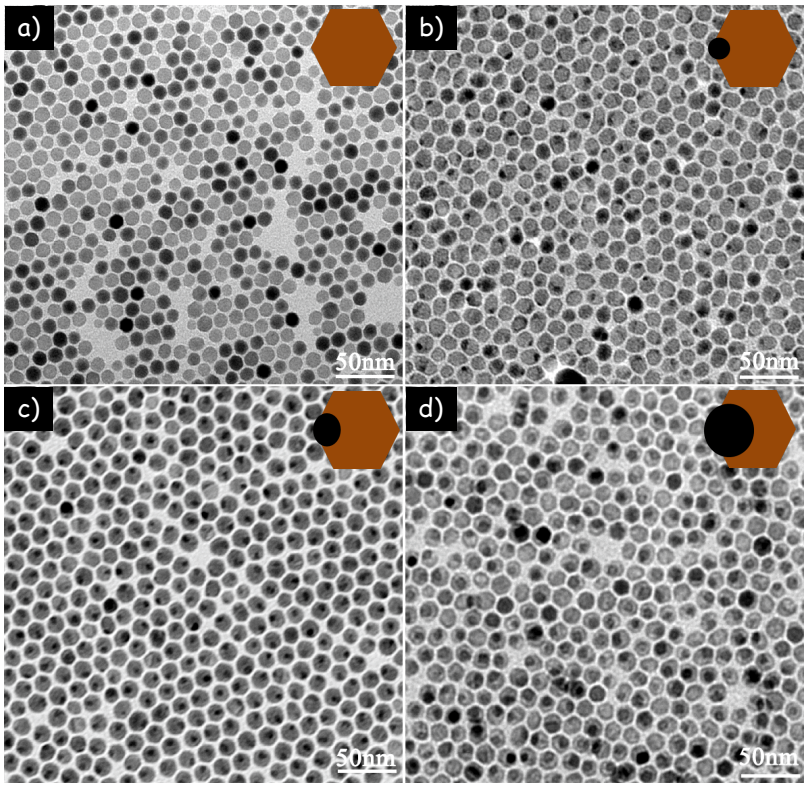

Figure 1. TEM images of CZTS nanocrystals (a) and CZTS-Ag_2S heterostructures with different amounts of $AgNO_3$ precursor: 0.4 mmol (b, Sample H1), 0.8 mmol (c, Sample H2), and 1.2 mmol (d, Sample H3)

XRD patterns of the CZTS nanocrystals before and after the addition of increasing amounts of Ag^+ cations are shown in Figure 2. Initial CZTS nanoparticles presented a wurtzite crystallographic structure.[37] As increasing amounts of Ag^+ were added, monoclinic Ag_2S (JCPDS card no. 14-0072) was formed, as it can be observed by the higher intensities of the peaks associated to Ag_2S crystallographic phase. Energy-dispersive x-ray spectroscopy (EDX) analysis (Table S1) verified the increasing ratio of [Ag]/[Cu+Zn+Sn] when increasing the amount of Ag^+ ions introduced. Further confirmation of the element oxidation states was obtained by XPS. Besides the existence of Cu, Zn, Sn, S, the XPS spectrum for both sample H1 and H3 (Figure S1) also showed the components at 368.0 and 374.0 eV, which were attributed to Ag $3d_{5/2}$ and Ag $3d_{3/2}$ of Ag^+ ions in the Ag_2S phase. Based on these results, we believe Cu, Zn and Sn atoms in CZTS behave virtually like a "fluid", which diffuses towards the solid-liquid interface through the anion sub-lattice and is replaced by Ag^+, with a slight preferential exchange of Zn^{2+} ions by Ag^+. The exchange is in part driven by the extremely small solubility constant of Ag^+, $K_{sp}=1.0\times10^{-49}$ at 18 °C.[38] The nanoparticle shape is conserved because of the lower activation barriers for the diffusion of smaller cations compared to anions, which sub-lattice integrity is conserved.

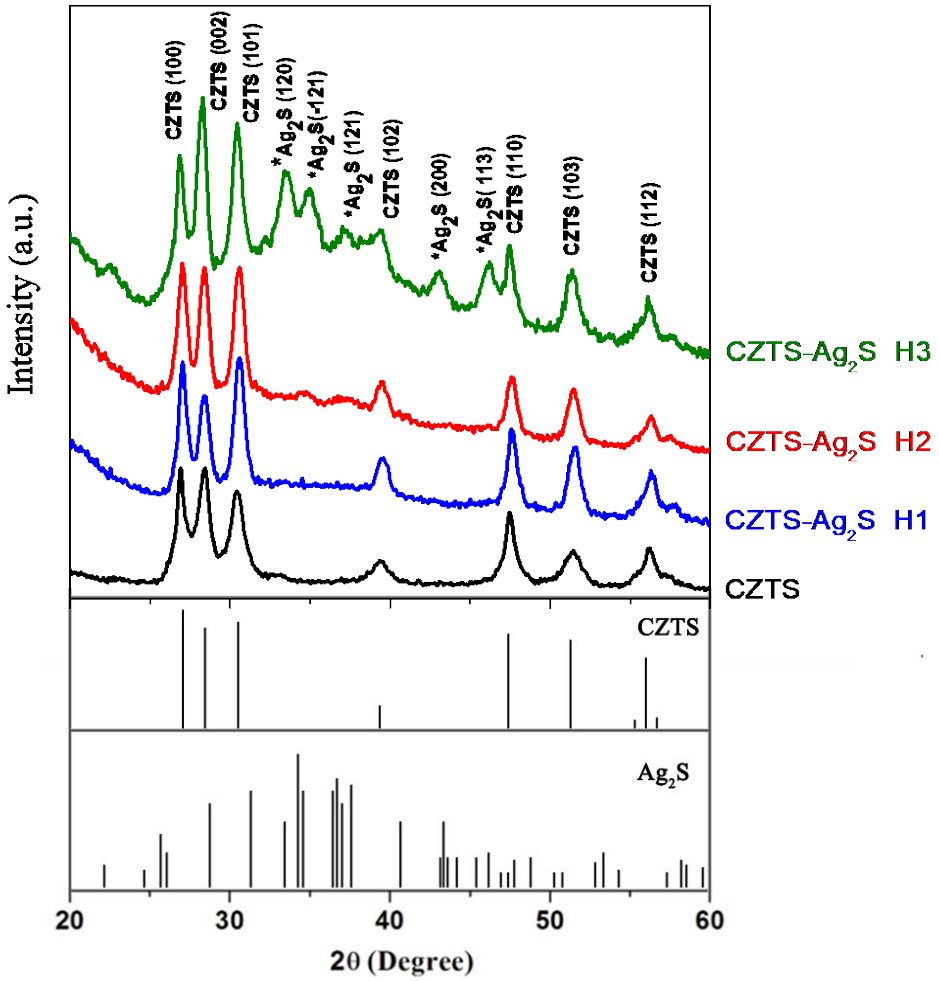

Figure 2. XRD patterns of CZTS nanocrystals and CZTS-Ag_2S nanoheterostructures obtained with the increasing amount of $AgNO_3$ added (H1: 0.4 mmol; H2: 0.8 mmol; H3: 1.2 mmol).

HRTEM analysis confirmed the crystallographic phase of both compounds within the CZTS-Ag_2S nano-heterostructure and allowed determining the structural relationship at the interface. Figure 3 shows TEM, HRTEM, fast Fourier transform (FFT), and simulated HRTEM images of CZTS-Ag_2S heterostructures. In Figure 3a, details of each crystal structure (CZTS in green and Ag_2S in red) are shown along with their corresponding power spectra (FFTs). The Ag_2S crystal is visualized along the [311] axis of its monoclinic phase, with lattice parameters a = 0.4127 nm, b

= 0.6699 nm, c = 0.7838 nm (space group = P21/c) and α = γ = 90° and β = 99.67°. Power spectrum of the CZTS crystal unambiguously revealed that it had a wurtzite phase visualized along its [11-2-3] axis and with lattice parameters of a = b = 0.3839 nm and c = 0.6339 nm (space group = P63mc). Figure 3b shows a close-up HRTEM micrograph of the CZTS-Ag_2S interface. Its corresponding FFT power spectrum reveals a possible epitaxial relationship with a certain misorientation and lattice mismatch. In Figure 3c, green circled diffraction spot belongs to the (10-11) plane of the wurtzite CZTS phase which has a d-spacing value of 0.2944 nm and red circled diffraction spot belongs to the (10-3) plane of monoclinic Ag_2S phase that has a d-spacing value of 0.2363 nm. For clarity, figure 3d shows the inverse FFT of selected diffraction spots. Although they are slightly misoriented and the lattice mismatch between them is about 20%, the inverse FFT image shows an epitaxial relationship where there are 3 Ag_2S planes for every 2 CZTS plane (marked with white parenthesis in the image, showing the expected misfit dislocations). Similar epitaxial relations were observed on CZTS-Au nano-heterostructures by N. Pradhan group.[39]

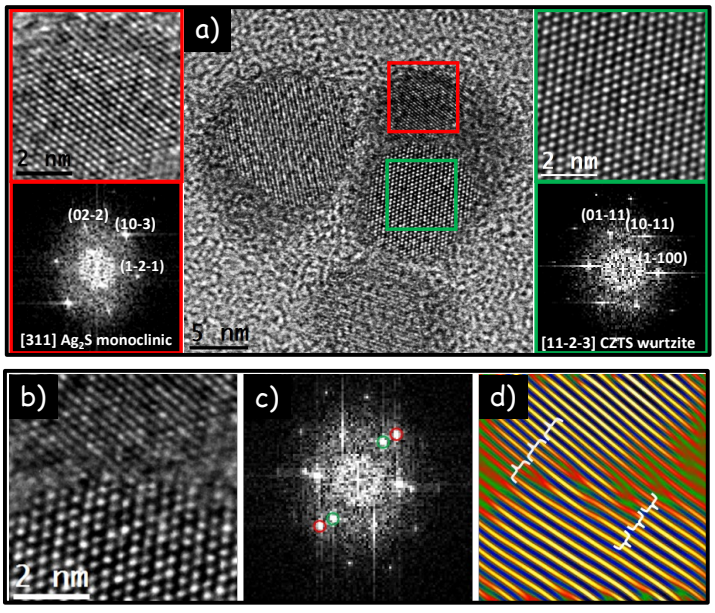

Figure 3. (a) HRTEM micrograph of CZTS-Ag_2S heterostructures. The closer look of the HRTEM image of CZTS and Ag_2S areas and its corresponding power spectrum analysis are shown in the left (Ag_2S, red) and right part (CZTS, green) panels, respectively. (b) HRTEM image of the interface between CZTS and Ag_2S within a single CZTS-Ag_2S nanoparticle. (c) The corresponding power spectrum, and (d) the inverse FFT of the circled diffraction spots showing the epitaxial relation.

As a proof-of-concept application, CZTS-Ag_2S nanoparticles were used as sensitizers in a photoelectrochemical cell (PEC) for water splitting. Within the PEC cell, electron-hole pairs are generated under visible light illumination. Photogenerated holes are used to oxidize H_2O and produce O_2 and the photogenerated electrons are driven towards the Pt electrode to produce hydrogen. As shown in Figure 4a, the photocurrent of TiO_2/CZTS-Ag_2S nanoheterostructures (H1) at 0.5 V is 0.15 mA/cm^2, what is much higher than that of the electrode made from pure TiO_2 (0.03 mA/cm^2) or that of the one incorporating CZTS nanocrystals (TiO_2/CZTS, 0.06 mA/cm^2). These values indicate that the CZTS-Ag_2S heterostructure promotes photocatalytic activity under visible light illumination. This result was further supported by the corresponding amperometric I–t cycles. Figure 4b shows the rapid and consistent photocurrent responses for each switch-on and -off event in multiple 10 second on–off cycles under visible-light illumination. The sample H2 showed the highest photocurrent density (ca. 0.58 mA/cm^2), which was about 10 times higher than that of the pure CZTS electrode (ca. 0.06 mA/cm^2). However, the photocurrent decreased when further increasing the amount of Ag_2S (sample H3). This indicates that an optimal compositional ratio of the two phases exist that provides the highest photocatalytic activity as will be discussed below.

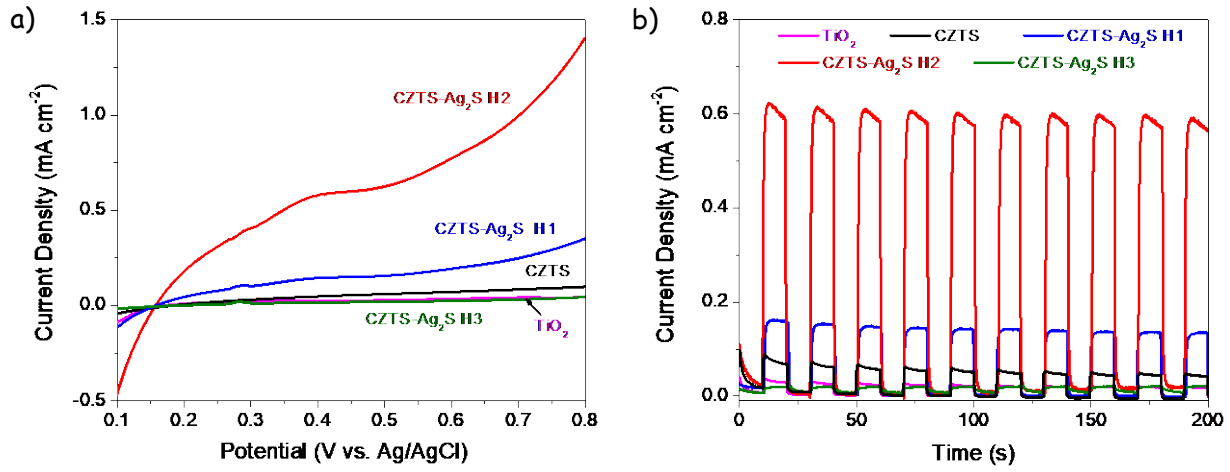

Figure 4. (a) Linear sweep voltammograms curves under visible light illumination for PECs. (b) The corresponding amperometric I–t curves under switching light ON-OFF at the applied potential of 0.5 V.

Main key parameters determining the PEC activity are charge carriers photogeneration, separation and transport efficiency.[40] To be able to account for the performance enhancement, light absorption and charge separation and transfer properties of the CZTS-Ag_2S (H2) heterostructures were studied. As shown in Figure S2, just a slight extension of the absorbance edge toward the infrared was observed after coupling CZTS (1.5 eV) with Ag_2S. This observation agrees well with the fact that 4 nm Ag_2S nanocrystals do not exhibit quantum confinement effects and thus possess a bulk-like band gap (~ 1.0 eV).[41] To better understand the electronic properties of CZTS-Ag_2S heterostructures, Mott-Sckottky (M-S) measurements were performed in dark using impedance spectroscopy. Figure S3 shows M-S plots of TiO_2 and CZTS-Ag_2S (H2) sensitized TiO_2. The flat band potential for TiO_2, calculated from the x intercept of the linear region, was found to be -0.8 V vs. Ag/AgCl. Just a slight positive shift of potential was found for the TiO_2-CZTS-Ag_2S sample. This sample was also characterized by a lower slope of the linear region, which suggested a much higher donor density. The energy band

structures of TiO_2, Ag_2S and CZTS are plotted in Figure 5a. The Fermi level in n-type TiO_2 and Ag_2S are close to their conduction band minimum (CBM), while that of p-type CZTS are close to its valence band maximum (VBM). As the CBM and VBM of p-type CZTS are situated at higher energy levels than Ag_2S,[42] under visible-light irradiation, photogenerated electrons in the CB of CZTS will transfer to the CB of Ag_2S, while holes travel in the opposite direction within the VB, as shown in Figure 5a. This type-II band alignment in the CZTS-Ag_2S nanoscale p-n heterostructure increases the driving force for photogenerated charge carrier separation, thus reducing the chance for their recombination, increasing their lifetime and enhancing the overall material photocatalytic performance.[43] Besides, the relatively low CBM of Ag_2S still facilitates the electron transfer to the CB of TiO_2. In a third step, as shown in Figure 5b, the efficiently separated electrons are collected on the surface of electrodes and injected into the external circuit, which are subsequently consumed in the reduction of water into hydrogen,[44] while holes participate in the oxidation reaction taking place at the CZTS surface.

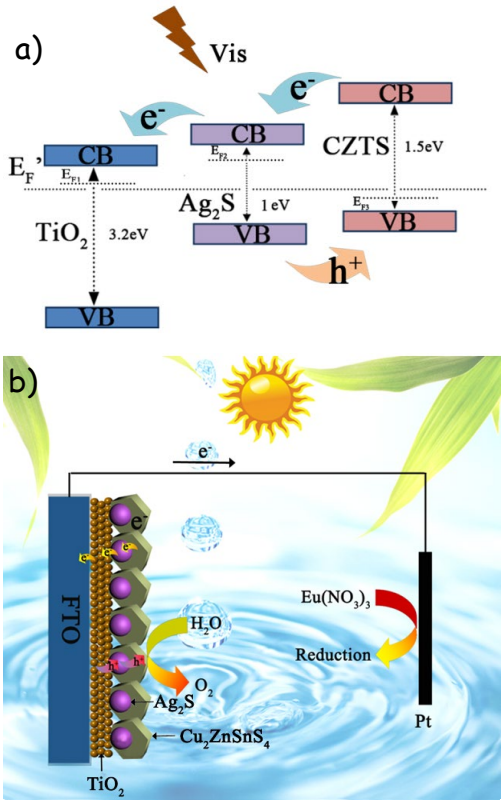

Figure 5. (a) Schematic of the energy band diagram of the heterostructures and the possible model of electron transfer. (b) Schematic diagram of water splitting reaction in the photoelectrochemical cell.

While the combination of CZTS and Ag_2S clearly results in an enhancement of the photocatalytic properties, it is also clear that an optimum composition exist. One possible explanation for the composition-dependent PEC activities measured might be ascribed to the structural change of CZTS in the presence of different concentration of Ag^+. Along with the increase of Ag^+ concentration, the molar ratio of Zn/(Cu+Sn) decreases from 0.32 to 0.17. As previously reported, the content of Zn can affect the CBM of the particles. In this direction, usually Zn-rich CZTS nanocrystals exhibit better photovoltaic conversion efficiency.[45-46] For CZTS-Ag_2S nano-heterostructures, a narrowing of the CZTS band gap from 1.5 to 1.37 eV was

observed when increasing the Ag+ concentration (Figure S4), what may difficult the transfer of electrons from CZTS to Ag_2S. A second explanation for the PEC activity decrease with the increase of Ag^+ is related to the loss of effective donors for the oxidation reaction. The decreased amount of CZTS with good hole transport ability results in a lower donor density. Furthermore, excessive Ag_2S in the heterostructures surface might reduce the CZTS reactive sites for the oxidation reaction, thus deteriorating the hole extraction from CZTS. This is consistence with the fact that, for type-II nanoparticles, the use of linear heterostructures is more favorable than the use of core-shells to extract charge from both semiconductor phases.[7d]

Conclusions

In summary, a series of CZTS–Ag_2S nanoscale p-n heterostructures with different CZTS/Ag_2S ratios was obtained by partial cation exchange. From HRTEM characterization, we conclude that the heterojunction has coincident site epitaxy. Such CZTS–Ag_2S nano-heterostructures exhibited significantly enhanced photoelectrochemical current response under visible-light illumination compared to pure CZTS. The ability to synthesize such structures with controlled composition and suitable band alignment promoting charge separation provides a better insight into fundamental synthetic chemistry as well as opening avenues for diverse optoelectronic applications.

AUTHOR INFORMATION

Corresponding Author

acabot@irec.cat

zyh@cugb.edu.cn

Notes

The authors declare no competing financial interest.

ACKNOWLEDGMENT

This work was supported by the European Regional Development Funds, the Framework 7 program under project SCALENANO (FP7-NMP-ENERGY-2011-284486), the Spanish MINECO under contract ENE2013-46624-C4-3-R and Fundamental Research Funds for the Central Universities (2652015086). Authors acknowledge the funding from Generalitat de Catalunya 2014 SGR 1638.

REFERENCES

(1) Zhang, H.; Jang, J.; Liu, W.; Talapin, D. V., Colloidal Nanocrystals with Inorganic Halide, Pseudohalide, and Halometallate Ligands. *ACS Nano* **2014**, *8*, 7359-7369.

(2) Zhang, L.; Xia, Y., Scaling up the Production of Colloidal Nanocrystals: Should We Increase or Decrease the Reaction Volume? *Adv. Mater.* **2014**, *26*, 2600-2606.

(3) Park, J.; An, K.; Hwang, Y.; Park, J.-G.; Noh, H.-J.; Kim, J.-Y.; Park, J.-H.; Hwang, N.-M.; Hyeon, T., Ultra-Large-Scale Syntheses of Monodisperse Nanocrystals. *Nat. Mater.* **2004**, *3*, 891-895.

(4) Reiss, P.; Bleuse, J.; Pron, A., Highly Luminescent CdSe/ZnSe Core/Shell Nanocrystals of Low Size Dispersion. *Nano Lett.* **2002**, *2*, 781-784.

(5) Li, L.; Daou, T. J.; Texier, I.; Kim Chi, T. T.; Liem, N. Q.; Reiss, P., Highly Luminescent $CuInS_2$/ZnS Core/Shell Nanocrystals: Cadmium-Free Quantum Dots for in Vivo Imaging. *Chem. Mater.* **2009**, *21*, 2422-2429.

(6) Lee, J.-S.; Bodnarchuk, M. I.; Shevchenko, E. V.; Talapin, D. V., "Magnet-in-the-Semiconductor" FePt−PbS and FePt−Pbse Nanostructures: Magnetic Properties, Charge Transport, and Magnetoresistance. *J. Am. Chem. Soc.* **2010**, *132*, 6382-6391.

(7) Zhao, Q.; Ji, M.; Qian, H.; Dai, B.; Weng, L.; Gui, J.; Zhang, J.; Ouyang, M.; Zhu, H., Controlling Structural Symmetry of a Hybrid Nanostructure and Its Effect on Efficient Photocatalytic Hydrogen Evolution. *Adv. Mater.* **2014**, *26*, 1387-1392.

(8) Chen, J.; Wu, X.; Yin, L.; Li B.; Hong X,; Fan, Z.; Chen, B.; Xue C.; Zhang, H., One-pot Synthesis of CdS Nanocrystals Hybridized with Single-Layer Transition-Metal Dichalcogenide Nanosheets for Efficient Photocatalytic Hydrogen Evolution. *Angew. Chem. Int. Ed.* **2015**, *54*, 1210-1214.

(9) Zhou, W.; Yin, Z.; Du, Y.; Huan, X.; Zeng, Z.; Fan, Z.; Liu, H.; Wang, J.; Zhang, H., Synthesis of Few-Layer MoS_2 Nanosheet-Coated TiO_2 Nanobelt Heterostructures for Enhanced Photocatalytic Activities, *Small*, **2013**, *9*, 140-147

(10) Ibáñez, M.; Zamani, R.; Gorsse, S.; Fan, J.; Ortega, S.; Cadavid, D.; Morante, J. R.; Arbiol, J.; Cabot, A., Core–Shell Nanoparticles as Building Blocks for the Bottom-up Production of Functional Nanocomposites: PbTe–PbS Thermoelectric Properties. *ACS Nano* **2013**, *7*, 2573-2586.

(11) Meng, F.; Li, J.; Cushing, S. K.; Zhi, M.; Wu, N., Solar Hydrogen Generation by Nanoscale P–N Junction of P-Type Molybdenum Disulfide/N-Type Nitrogen-Doped Reduced Graphene Oxide. *J. Am. Chem. Soc.* **2013**, *135*, 10286-10289.

(12) Kumar, S.; Jones, M.; Lo, S. S.; Scholes, G. D., Nanorod Heterostructures Showing Photoinduced Charge Separation. *Small* **2007**, *3*, 1633-1639.

(13) Steiner, D.; Dorfs, D.; Banin, U.; Della Sala, F.; Manna, L.; Millo, O., Determination of Band Offsets in Heterostructured Colloidal Nanorods Using Scanning Tunneling Spectroscopy. *Nano Lett.* **2008**, *8*, 2954-2958.

(14) Rivest, J. B.; Swisher, S. L.; Fong, L.-K.; Zheng, H.; Alivisatos, A. P., Assembled

Monolayer Nanorod Heterojunctions. *ACS Nano* **2011**, *5*, 3811-3816.

(15) Teranishi, T.; Sakamoto, M., Charge Separation in Type-II Semiconductor Heterodimers. *J. Phys. Chem. Lett.* **2013**, *4*, 2867-2873.

(16) Rivest, J. B.; Jain, P. K., Cation Exchange on the Nanoscale: An Emerging Technique for New Material Synthesis, Device Fabrication, and Chemical Sensing. *Chem. Soc. Rev.* **2013**, *42*, 89-96.

(17) Son, D. H.; Hughes, S. M.; Yin, Y.; Alivisatos, A. P., Cation Exchange Reactions in Ionic Nanocrystals. *Science* **2004**, *306*, 1009-1012.

(18) De Trizio, L.; Li, H.; Casu, A.; Genovese, A.; Sathya, A.; Messina, G. C.; Manna, L., Sn Cation Valency Dependence in Cation Exchange Reactions Involving $Cu_{2-X}Se$ Nanocrystals. *J. Am. Chem. Soc.* **2014**, *136*, 16277-16284.

(19) Bera, A.; Dey, S.; Pal, A. J., Band Mapping across a PN-Junction in a Nanorod by Scanning Tunneling Microscopy. *Nano Lett.* **2014**, *14*, 2000-2005.

(20) Wu, X. J.; Huang, X.; Qi, X.; Li, H.; Li, B.; Zhang, H., Copper-Based Ternary and Quaternary Semiconductor Nanoplates: Templated Synthesis, Characterization, and Photoelectrochemical Properties. *Angew. Chem. Int. Ed.* **2014**, *126*, 9075-9079.

(21) De Trizio, L.; Gaspari, R.; Bertoni, G.; Kriegel, I.; Moretti, L.; Scotognella, F.; Maserati, L.; Zhang, Y.; Messina, G. C.; Prato, M., $Cu_{3-X}P$ Nanocrystals as a Material Platform for near-Infrared Plasmonics and Cation Exchange Reactions. *Chem. Mater.* **2015**, *27*, 1120-1128.

(22) Lesnyak, V.; George, C.; Genovese, A.; Prato, M.; Casu, A.; Ayyappan, S.; Scarpellini, A.; Manna, L., Alloyed Copper Chalcogenide Nanoplatelets Via Partial Cation Exchange Reactions. *ACS Nano* **2014**, *8*, 8407-8418.

(23) Park, Y.; McDonald, K. J.; Choi, K.-S., Progress in Bismuth Vanadate Photoanodes for Use

in Solar Water Oxidation. *Chem. Soc. Rev.* **2013**, *42*, 2321-2337.

(24) Ha, E.; Lee, L. Y. S.; Wang, J.; Li, F.; Wong, K. Y.; Tsang, S. C. E., Significant Enhancement in Photocatalytic Reduction of Water to Hydrogen by Au/Cu_2ZnSnS_4 Nanostructure. *Adv. Mater.* **2014**, *26*, 3496-3500.

(25) Yu, X.; Shavel, A.; An, X.; Luo, Z.; Ibáñez, M.; Cabot, A., Cu_2ZnSnS_4-Pt and Cu_2ZnSnS_4-Au Heterostructured Nanoparticles for Photocatalytic Water Splitting and Pollutant Degradation. *J. Am. Chem. Soc.* **2014**, *136*, 9236-9239.

(26) Moriya, M.; Minegishi, T.; Kumagai, H.; Katayama, M.; Kubota, J.; Domen, K., Stable Hydrogen Evolution from CdS-Modified $CuGaSe_2$ Photoelectrode under Visible-Light Irradiation. *J. Am. Chem. Soc.* **2013**, *135*, 3733-3735.

(27) Patrick, D.; Malinda, R.; Brittany, H.; Michelle, T.; Javier, V., Cu_2ZnSnS_4−Au Heterostructures: Toward Greener Chalcogenide Based Photocatalysts, *J. Phys. Chem. C* **2014**, *118*, 21226-21234.

(28) Priya, K.; Kalyanjyoti, D.; Anup, K.; Sasanka, D., Efficient Hydrogen/Oxygen Evolution and Photocatalytic Dye Degradation and Reduction of Aqueous Cr(VI) by Surfactant Free Hydrophilic Cu_2ZnSnS_4 Nanoparticles, *J. Phys. Chem. C*, **2014**, *118*, 21226-21234.

(29) Shavel, A.; Cadavid, D.; Ibanez, M.; Carrete, A.; Cabot, A., Continuous Production of Cu_2ZnSnS_4 Nanocrystals in a Flow Reactor. *J. Am. Chem. Soc.* **2012**, *134*, 1438-1441.

(30) Singh, A.; Geaney, H.; Laffir, F.; Ryan, K. M., Colloidal Synthesis of Wurtzite Cu_2ZnSnS_4 Nanorods and Their Perpendicular Assembly. *J. Am. Chem. Soc.* **2012**, *134*, 2910-2913.

(31) Singh, A.; Singh, S.; Levcenko, S.; Unold, T.; Laffir, F.; Ryan, K. M., Compositionally Tunable Photoluminescence Emission in $Cu_2ZnSn\ (S_{1-X}Se_X)_4$ Nanocrystals. *Angew. Chem. Int. Ed.* **2013**, *52*, 9120-9124.

(32) Ibáñez, M.; Zamani, R.; Li, W.; Shavel, A.; Arbiol, J.; Morante, J. R.; Cabot, A., Extending the Nanocrystal Synthesis Control to Quaternary Compositions. *Cryst. Growth Des.* **2012**, *12*, 1085-1090.

(33) Ibáñez, M.; Zamani, R.; Li, W.; Cadavid, D.; Gorsse, S.; Katcho, N. A.; Shavel, A.; López, A. M.; Morante, J. R.; Arbiol, J., Crystallographic Control at the Nanoscale to Enhance Functionality: Polytypic Cu_2GeSe_3 Nanoparticles as Thermoelectric Materials. *Chem. Mater.* **2012**, *24*, 4615-4622.

(34) Ibáñez, M.; Cadavid, D.; Zamani, R.; García-Castelló, N.; Izquierdo-Roca, V.; Li, W.; Fairbrother, A.; Prades, J. D.; Shavel, A.; Arbiol, J., Composition Control and Thermoelectric Properties of Quaternary Chalcogenide Nanocrystals: The Case of Stannite $Cu_2CdSnSe_4$. *Chem. Mater.* **2012**, *24*, 562-570.

(35) Ibáñez, M.; Zamani, R.; LaLonde, A.; Cadavid, D.; Li, W.; Shavel, A.; Arbiol, J.; Morante, J. R.; Gorsse, S.; Snyder, G. J., $Cu_2ZnGeSe_4$ Nanocrystals: Synthesis and Thermoelectric Properties. *J. Am. Chem. Soc.* **2012**, *134*, 4060-4063.

(36) Gupta, S.; Kershaw, S. V.; Rogach, A. L., 25th Anniversary Article: Ion Exchange in Colloidal Nanocrystals. *Adv. Mater.* **2013**, *25*, 6923-6944.

(37) Lu, X.; Zhuang, Z.; Peng, Q.; Li, Y., Wurtzite Cu_2ZnSnS_4 Nanocrystals: A Novel Quaternary Semiconductor. *Chem. Commun.* **2011**, *47*, 3141-3143.

(38) Pang, M.; Hu, J.; Zeng, H. C., Synthesis, Morphological Control, and Antibacterial Properties of Hollow/Solid Ag_2S/Ag Heterodimers. *J. Am. Chem. Soc.* **2010**, *132*, 10771-10785.

(39) Patra, B. K.; Shit, A.; Guria, A. K.; Sarkar, S.; Prusty, G.; Pradhan, N., Coincident Site Epitaxy at the Junction of Au–Cu_2ZnSnS_4 Heteronanostructures. *Chem. Mater.* **2015**, *27*, 650-657.

(40) Liu, J.; Yu, X.; Liu, Q.; Liu, R.; Shang, X.; Zhang, S.; Li, W.; Zheng, W.; Zhang, G.; Cao, H., Surface-Phase Junctions of Branched TiO_2 Nanorod Arrays for Efficient Photoelectrochemical Water Splitting. *Appl. Catal. B: Environ.* **2014**, *158*, 296-300.

(41) Huxter, V. M.; Mirkovic, T.; Nair, P. S.; Scholes, G. D., Demonstration of Bulk Semiconductor Optical Properties in Processable Ag_2S and Eus Nanocrystalline Systems. *Adv. Mater.* **2008**, *20*, 2439-2443.

(42) Yang, X.; Xue, H.; Xu, J.; Huang, X.; Zhang, J.; Tang, Y.-B.; Ng, T.-W.; Kwong, H.-L.; Meng, X.-M.; Lee, C.-S., Synthesis of Porous Zns: Ag_2S Nanosheets by Ion Exchange for Photocatalytic H_2 Generation. *ACS Appl. Mater. Interfaces* **2014**, *6*, 9078-9084.

(43) Gao, X.; Wu, H. B.; Zheng, L.; Zhong, Y.; Hu, Y.; Lou, X. W. D., Formation of Mesoporous Heterostructured $BiVO_4/Bi_2S_3$ Hollow Discoids with Enhanced Photoactivity. *Angew. Chem. Int. Ed.* **2014**, *126*, 6027-6031.

(44) Shen, H.; Jiao, X.; Oron, D.; Li, J.; Lin, H., Efficient Electron Injection in Non-Toxic Silver Sulfide (Ag_2S) Sensitized Solar Cells. *J. Power Sources* **2013**, *240*, 8-13.

(45) Riha, S. C.; Fredrick, S. J.; Sambur, J. B.; Liu, Y.; Prieto, A. L.; Parkinson, B., Photoelectrochemical Characterization of Nanocrystalline Thin-Film Cu_2ZnSnS_4 Photocathodes. *ACS Appl. Mater. Interfaces* **2010**, *3*, 58-66.

(46) Wang, Y.-X.; Wei, M.; Fan, F.-J.; Zhuang, T.-T.; Wu, L.; Yu, S.-H.; Zhu, C.-F., Phase-Selective Synthesis of Cu_2ZnSnS_4 Nanocrystals through Cation Exchange for Photovoltaic Devices. *Chem. Mater.* **2014**, *26*, 5492-5498.

TOC